# Nearly Total Omnidirectional Reflection by a Single Layer of Nanorods

Junjie Du, Zhifang Lin, S. T. Chui, Guangjiong Dong, and Weiping Zhang

Phys. Rev. Lett. **110**, 163902 — Published 18 April 2013

DOI: 10.1103/PhysRevLett.110.163902

# Nearly Total, Omnidirectional Reflection by a Single Layer of Nanorods

Junjie Du,[1,2,*] Zhifang Lin,[3] S. T. Chui,[4] Guangjiong Dong,[1,2] and Weiping Zhang[1,2,†]

[1] *Quantum Institute for Light and Atoms, East China Normal University, Shanghai 200062, China*
[2] *Department of Physics, State Key Laboratory of Precision Spectroscopy, East China Normal University, Shanghai 200062, China*
[3] *Key Laboratory of Micro and Nano Photonic Structures (Ministry of Education), Fudan University, Shanghai, China*
[4] *Bartol Research Institute and Department of Physics and Astronomy, University of Delaware, Newark, DE 19716, USA*

It is shown that a single-layer array of high electric permittivity (high-$\varepsilon$) rods with radius smaller than $\lambda/10$ is capable of reflecting more than 97% of the energy of optical waves with arbitrary incident angle. Here $\lambda$ is the incident wavelength. The occurrence of the phenomenon depends on the construction of two particular grating modes (GMs) in the array which result in two corresponding transmitted wave components that cancel each other. The construction of the dominant GMs in the array benefits from the highly independent manipulability of the angular momenta components with opposite signs in high-$\varepsilon$ particles. The effect offers a possibility for improving the optical elements integration level in the on-chip optical circuits.

PACS numbers: 41.20.Jb, 78.20.Ci 42.25.Fx 73.20.Mf

In current integration of optics and phononics, as well as in micro/nano-fluid mechanics, there is a strong quest for exploring new mechanisms of manipulating electromagnetic(EM), sonic and water waves with miniaturized subwavelength structures. Single-particle-layer structures have been suggested to shrink the size of devices and remarkable progress has been made in optics based on the nonlinear effect[1, 2], the phase shift produced by resonant particles[3–5], the coupling between plasmonic coaxial waveguides[6] and the symmetry of resonant modes of particles[7]. Even graphene with one-atom thickness is applied to guide the flow of light[8, 9]. Besides ultrathin thickness much smaller than the wavelength, they have the negligible absorption loss at the same time since few materials are involved. It is therefore expected that single-layer structures can achieve more applications in optical manipulation by exploring and utilizing their exotic properties.

Recently the single-particle-layer array has been employed to develop a reflector which can highly reflect the EM waves with a particular incident angle[10–13]. The realization of high reflectivity depends on the utilization of dielectric particles with high permittivity ($\varepsilon$) which is available in some semiconductor materials such as $FeS_2$ whose $\varepsilon$ has a real part much larger than 20 and a negligible imaginary part [14] at optical frequencies. Moreover, the recent development of metamaterials makes it possible to obtain seemingly arbitrary effective permittivity and permeability theoretically[15]. This attracts us to pay attention to the following fascinating optical properties of high-$\varepsilon$ particles: (1) Subwavelength scattering resonance. For example, when the conditions of scattering resonant state of constituent particles and the separation smaller than $\lambda/2$[16–21] are required simultaneously, particles with high $\varepsilon$ offer a way to fulfill all the requirements. (2) Strong field inside the particles. The strong field inside high-$\varepsilon$ dielectric effectively produces an electric dipole or multipole that is tunable by the inter-particle coupling.

Up to now, the application of all the single-layer reflectors is hampered by the limitation in the angle of incidence, in comparison with the photonic crystal counterparts [22–24] which enable EM waves of arbitrary angle of incidence to be reflected with low absorption loss at the infrared and optical frequencies. However, the single-layer feature still makes it show great potential in the miniaturization of devices. In this Letter, we propose a theoretical design in which EM wave with arbitrary incident angle can be highly reflected by a single-layer rod array that has subwavelength thickness with the rod radius $r_s$ smaller than 1/10 of the incident wavelength $\lambda$. Since the inter-rod separation $a_0$ is smaller than $\lambda/2$, the array can be seen as a zeroth-order grating composed of high-$\varepsilon$ rods which have the property (2) and are between two subwavelength resonant states. Despite the existence of the inter-rod gap, we show that the structure has abilities to inhibit the wave of arbitrary incident angle penetrating through itself due to the diffraction effect as long as $\varepsilon$ of rods is larger than 20. The single-layer array behaves as a fence that safeguards against the EM waves. The compact design probably makes it extremely appealing in the on-chip optical architecture.

Let us start by considering two-dimensional circular rods of permittivity $\varepsilon_s = 20$ with radius $r_s$ set as the unit of length. The rods are uniform in the $z$ direction and are arrayed into a line in the $y$ direction with the separation $a_0 = 2.67r_s = 2.67$. The reflectivity is shown in Fig. 1 (a) when the magnetic field of a Gaussian beam is polarized along the rod axis. Here the calculation is carried out using the rigorous multiple scattering theory[7]. The near-100% reflection occurs when the reduced frequency $\omega a_0/2\pi c$ is around 0.259 for arbitrary

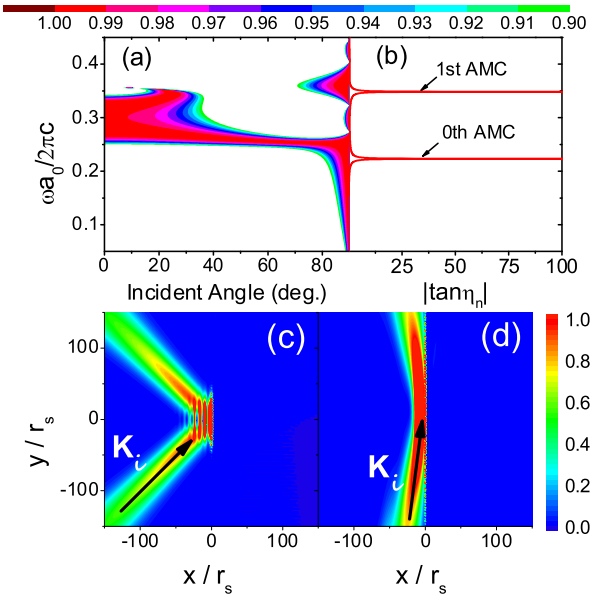


FIG. 1: (color online) (a) The reflectivity versus reduced frequency $\omega a_0/2\pi c$ and angle of incidence for the single-layer array of rods described in the text. (b) $|\tan\eta_n|$ versus frequency for a single rod with radius $r_s$=1. The peaks denote the 0th and 1st AMC resonances. Distribution of the H field intensity when a Gaussian beam strikes a single-layer array in the $y$ direction at $\theta_i = 45°$ (c) and 80° (d).

angle of incidence $\theta_i$ from 0° to 90°, where $\omega$ is angular frequency and $c$ is the speed of light in the vacuum. This means that the inter-rod separation $a_0 \approx 0.26\lambda$ and the rod radius $r_s \lesssim 0.1\lambda$. As a result, the thickness of the single-layer is as thin as 1/5 of the incident wavelength. The wider frequency band of near-100% reflection can be achieved by using the dielectric rods with higher $\varepsilon$. Typically, here we show the total reflection of a beam with $\theta_i = 45°$ and 80° in Figs. 1(c) and (d), respectively. The resonance spectrum of the single rod is plotted in Fig. 1 (b) using the Mie scattering theory[25] in which the incoming and scattered magnetic (H) fields are expanded as $H_i = \sum_n i^n p_n J_n(k_b r) e^{in\phi}$ and $H_s = \sum_n i^n b_n H_n^{(1)}(k_b r) e^{in\phi}$. Here $r$ and $\phi$ are the polar coordinates, $J_n$ and $H_n^{(1)}$ are, respectively, the $n$th order Bessel function and Hankel function of the first kind and $k_b$ is the wave numder in the background medium. The $n$ in summation $\sum_n$ runs from $-\infty$ to $+\infty$ with the $n$th term in the summation denoting the $n$th angular momentum channel (AMC). The Mie scattering coefficient $\alpha_n$ can be written as $\alpha_n = -1/(1 + i\cot\eta_n)$ with $\eta_n$ being the scattering phase shift of the $n$th AMC. The peaks of $|\tan\eta_n|$ versus frequency, as shown in Fig. 1(b), correspond to the Mie resonance of a single rod in different AMCs [25, 26].

Since the frequency band of the total reflection lies between the first and second resonant states of the single rod, three angular momenta components $n = 0$, $+1$ and $-1$ contribute the most to the all-angle total reflection. For an isolated rod, the component $n = 0$ corresponds to an isotropic inner and scattered field[7]. Usually the summation of two components $n = +1$ and $-1$ is called as the 1st AMC with its inner and scattered field having dipolar symmetry[7, 25]. However, each of the two components receives little attention separately. Fig. 2 shows that the $n = -1$ and the $n = +1$ component denotes a clockwise and an anti-clockwise rotating dipole moment, respectively, which manifests itself by a finite vortex of energy flow in Figs. 2 (a) and (b). Because $b_{-1} = b_1$ for an isolated isotropic rod, two rotating dipole moments have the same amplitude and the definite phase difference. Their superposition will result in a linear oscillating dipole as shown in Fig. 2 (c). Fig. 2(f) shows that a dipole-like scattered field from an linear oscillating dipole is produced by the superposition of the scattered field in the $-1$st component in Fig. 2(d) and that in the $+1$st component in Fig. 2(e)[25]. This somewhat resembles a linearly polarized wave that is the superposition of a left-circularly and a right-circularly polarized wave. When the rod has high $\varepsilon$, the effective electric dipole will have induced charge of high magnitude which strengthens the inter-rod interaction. Therefore, unlike the usual case in which the components $+1$ and $-1$ behave as a whole, in a one-dimensional rod chain angular momenta components of opposite signs can be independently manipulated. The tunability feature helps to construct the particular grating modes (GMs) in the chain. Furthermore, the transmitted wave components from different GMs interfere destructively, leading to the occurrence of the near-100% reflection.

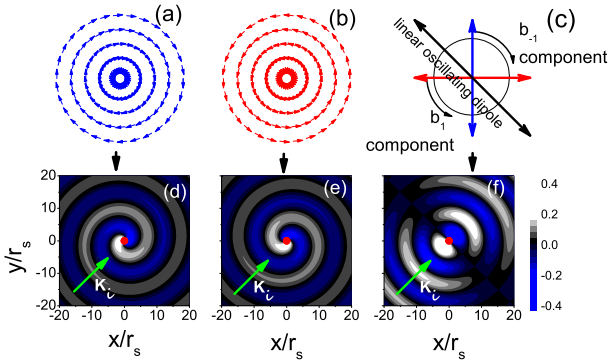


FIG. 2: (color online) The time-averaged Poynting vector inside an isolated rod in the $-1$st (a) and the $+1$st (b) AMC, showing a vortex of energy flow and implying a rotating dipole excited in rods. (c) The schematic diagram of the superposition of the anti-clockwise and clockwise rotating dipolar momentums to produce a linear oscillating dipolar momentum. The scattered field in the $-1$st (d) and the $+1$st (e) AMC. (f) The summation of the scattered fields in the $-1$st and the $+1$st AMC. The gray(red) circle denotes the rod.

We first analyze the role of the various GMs in the near-100% reflection. In order to analytically calculate

the GMs, we study an array which is composed of rods of square cross section since the underlying physics is independent on the shape of cross section of rods. The length of the side of the square is $s = 1.87$ and the separation and the wavelength are same as in Figs. 1(c) and (d). The transcendental equation governing the GMs [27, 28] in the array is

$$\cos k_m^b g \cos k_m^s s - \frac{1}{2}\left(\frac{\varepsilon_s k_m^b}{\varepsilon_b k_m^s} + \frac{\varepsilon_b k_m^s}{\varepsilon_s k_m^b}\right) \sin k_m^b g \sin k_m^s s = \cos k_y a_0, \quad (1)$$

where $g = a_0 - s$, $k_m^b$ and $k_m^s$ are the longitudinal (parallel to the chain axis) wave vectors of the $m$th GM inside the gaps and rods. When combined with the condition

$$(2\pi/\lambda)^2 - (k_m^b)^2 = (2\pi/\lambda)^2 \varepsilon_s - (k_m^s)^2, \quad (2)$$

which implies that the transverse(perpendicular to the chain axis) wave vectors are equal in the gaps and rods, Eq. (1) gives out the eigenvalues $k_m^b$ and $k_m^s$ of different GMs[29, 30]. The GMs is responsible to transfer energy from the incident side to the transmission side. Let $t_m$ denote the contribution of the $m$th GM to transmission, the transmitted wave of the array can be expressed as

$$H_t(r) = \sum_{m=1}^{+\infty} t_m e^{i(k_y y + k_x (x - s/2))}. \quad (3)$$

Fig. 3(a) shows the transmitted wave components from the 1st and the 2nd GM along the line $y = 0$ for $\theta_i = 0°$ since the first two GMs dominate the phenomenon. The case of $\theta_i = 80°$ is given in Fig. 3(b). We see that two transmitted wave components away from the rods have a phase difference of $\pi$ and interfere destructively[29, 30], resulting in the near-100% reflection. This shows that we need the GMs which can produce the transmitted wave components of destructive interference at arbitrary $\theta_i$.

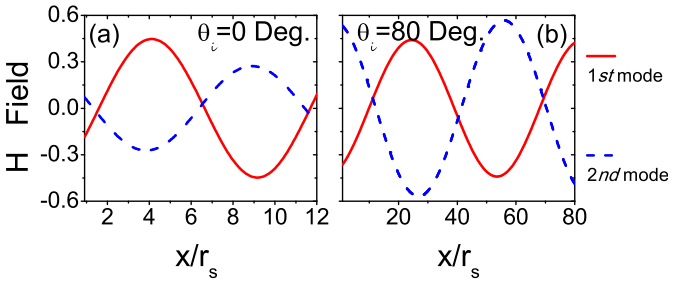


FIG. 3: (color online) The transmitted wave components originating from the 1st and the 2nd GMs when $\theta_i = 0°$ (a) and 80° (b).

Physically, the variation of $k_m^b$ and $k_m^s$ implies that the effective refractive indexes of the array are different in the different GMs[31]. Therefore, the two transmitted wave components can be out of phase as shown in Fig. 3.

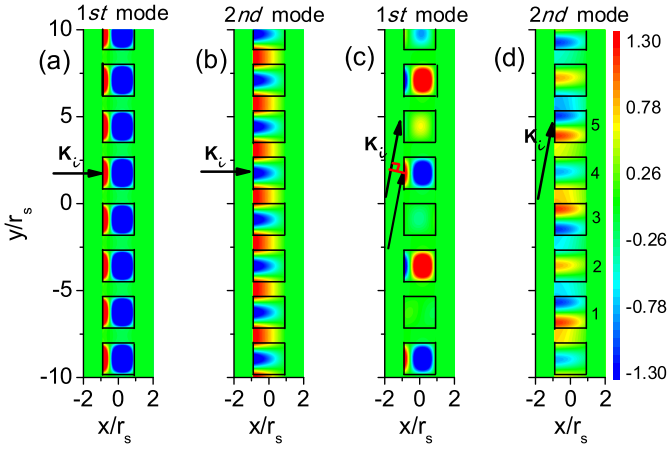


FIG. 4: (color online) The magnetic field distribution for the 1st (a) and the 2nd (b) GM inside the array for $\theta_i = 0°$. (c) and (d) correspond to the case of $\theta_i = 80°$. The rods are represented by the square.

In order to uncover the underlying physics, below we pay more attention to the formation mechanism of GMs by analyzing their distribution feature rather than the numerical value of the effective refractive index. Figs. 4(a) and (b) display the 1st and the 2nd GM inside the array, respectively, for $\theta_i = 0°$. For the 1st GM, Fig. 4(a) shows the H field inside the rod has dipolar symmetry. Correspondingly, the electric dipole moments inside the rods are aligned with the chain axis[7, 32, 33], so the mode is called as the longitudinal (L) mode. The 2nd GM in Fig. 4(b) is a typical standing wave mode along the chain axis with the adjacent nodes located near two sides of square rod perpendicular to the chain axis. In order to demonstrate the variation of modes when $\theta_i$ increases, we plot the first two GMs for $\theta_i = 80°$ in Figs. 4(c) and (d). The difference of the field modes between the adjacent rods in Figs. 4(c) and (d) is caused by the phase difference of the incident wave. The 1st GM is kept to be a L mode when $\theta_i$ increases to 80°, as observed in Figs. 4(a) and (c). However, the 2nd GM in Fig. 4(d) is strictly different from that in Fig. 4(b). The dipolar symmetry of the H field along the chain axis is induced inside the rod, and thus a transverse (T) mode is constructed[7, 32, 33]. It shows that the GMs should be tunable by varying $\theta_i$ in order to achieve the all-angle total reflection.

Next we will illustrate why the GMs can be tuned through $\theta_i$ with the help of three angular momenta components of rods. We will again study the circular rod as have being done in Fig. 2 and analyze its field modes of different angular momenta components since its scattering problem can be rigorously carried out. In Fig. 5 (a), three Mie scattering coefficients of a rod located in the array versus angle of incidence are given. The difference between $b_{-1}$ and $b_1$ gradually increases with $\theta_i$ increasing in Fig. 5 (b). For an isolated rod, this non-symmetric nature of angular momenta components of opposite signs $\pm n$

usually only occurs in anisotropic rods[34] and has been used to achieve an unidirectional EM edge states[35–38]. Now since $|b_1| < |b_{-1}|$, after the superposition they produce a clockwise rotating dipole moment inside the rod as shown in Fig. 5 (c). Accordingly, when $\theta_i$ increases from 45° to 80°, we see that the scattered field in the 1st AMC becomes more and more similar to that in the −1st AMC in Fig. 2 (d), by a comparison between Figs. 5 (d) and (e). It shows that the optical behavior of angular momenta components of opposite signs is not symmetrical when this rod is located in a one-dimensional array and can be independently manipulated when its $\varepsilon$ is high enough. This nature of the high-$\varepsilon$ rod provides a basis for the tunability of the GMs in the rod array. The resultant rotating dipole moment in Fig. 5 (c) inside the rod shows the array simultaneously supports the L and T modes since the rotating dipole moment is formed by the interaction of the two modes. Therefore, it is the independent manipulation of the +1st and the −1st AMC in high-$\varepsilon$ rods that makes the GMs tunable through $\theta_i$.

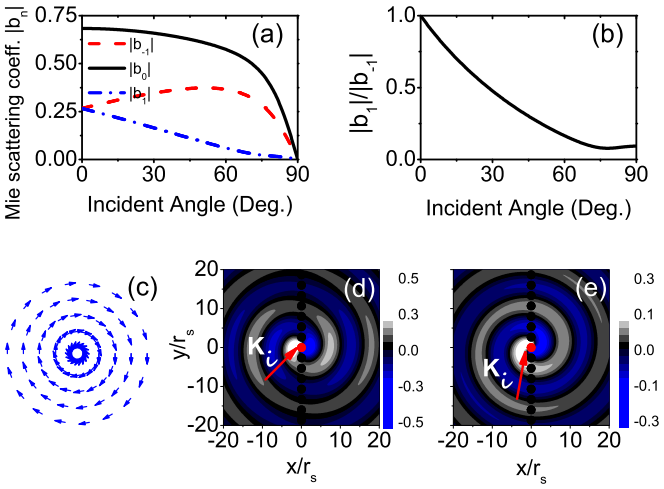


FIG. 5: (color online) (a) Mie scattering coefficients $b_{-1}$, $b_0$ and $b_1$ versus $\theta_i$ for a rod located in the array. (b) The ratio of $b_1$ to $b_{-1}$ with $\theta_i$ increasing. (c) The time-averaged Poynting vector inside a rod located in the array. The scattered field in the 1st AMC of a rod located in the array for $\theta_i = 45°$ (d) and $\theta_i = 80°$ (e). The scattered fields are calculated for the rod [gray(red)] located in the origin of coordinates. The presence of many rods in (d) and (e) implies the interrod coupling is considered compared to the case in Fig.2 (f).

Compared to the L mode which always can be excited for arbitrary angle of incidence, the T mode needs the gradual loss of $b_1$. From the viewpoint of mechanical system, the L mode is more stable and therefore easier to be excited since the adjacent electric dipole moments oriented along the chain axis have the weak interaction. It should be noted that the 0th AMC of rods also has an effect on the construction of GMs. For instance, The standing wave mode in Fig. 3 (b) is mainly supported by the 0th AMC. In addition, both the L mode with non-perfect dipolar symmetry in Figs. 4(a) and (c) and the states 2 and 4 in the T mode show the existence of the 0th AMC. However, though the working frequency is closer to the 0th AMC resonance, the 0th AMC can not be manipulated by the incident angle due to its isotropic symmetry and the all-angle total reflection must mainly depend on the 1st AMC.

In summary, we have shown that the all-angle nearly total reflection is possible using a single-layer array of high-$\varepsilon$ dielectric rods. The phenomenon is expected to find applications in designing compact optical components in photonic circuits. Our discussion applies equally to other classical waves and particularly to acoustic waves.

This work was supported by the China-973 Program (2011CB921604, 2011CB922004), NSFC (11104305, 11234003, 11129402, 11174059), and MOE of China (B06011). S. T. Chui is partly supported by the US DOE.

* Electronic address: phyjunjie@gmail.com
† Electronic address: wpzhang@phy.ecnu.edu.cn

[1] J. B. Pendry, Science **322**, 71, (2008).
[2] A. Aubry and J. B. Pendry, J. Opt. Soc. Am. B **27**, 72 (2010).
[3] D. Fattal, J. J. Li, Z. Peng, M. Fiorentino and R. G. Beausoleil, Nature Photon. **4**, 466 (2010).
[4] N. Yu, P. Genevet, M. A. Kats, F. Aieta, J. P. Tetienne, F. Capasso, and Z. Gaburro, Science **334**, 333 (2011).
[5] X. Ni, N. K. Emani, A. V. Kildishev, A. Boltasseva, and V. M. Shalaev, Science **335**, 427 (2012).
[6] S. P. Burgos, R. Waele, A. Polman, and H. A. Atwater, Nature Mater. **9**, 407 (2010).
[7] J. J. Du, Z. F. Lin, S. T. Chui, W. L. Lu, H. Li, A. Wu, Z. Sheng, J. Zi, X. Wang, S. Zou, and F. Gan, Phys. Rev. Lett. **106**, 203903 (2011).
[8] A. Vakil and N. Engheta, Science **332**, 1291, (2011).
[9] M. Liu, X. Yin, E. Ulin-Avila, B. Geng, T. Zentgraf, L. Ju, F. Wang, and X. Zhang, Nature **64**, 474, (2011).
[10] A. B. Evlyukhin, C. Reinhardt, A. Seidel, B. S. Luk'yanchuk, and B. N. Chichkov, Phys. Rev. B **82**, 045404 (2010).
[11] C. Chang-Hasnain, Semicond. Sci. Technol. **26**, 014043 (2011).
[12] M. Huang, Y. Zhou, and C. Chang-Hasnain, Nat. Photonics **1**, 119 (2007).
[13] R. Gomez-Medina, M. Laroche, and J. J. Saenz, Opt. Express **14**, 3730 (2006).
[14] E. D. Palic, *Handbook of Optical Constants in Solids*, (Academic, New York, 1985).
[15] D. R. Smith, J. B. Pendry, and M. C. K. Wiltshire, Science, **305**, 788 (2004).
[16] J. A. Schuller, R. Zia, T. Taubner, and M. L. Brongersma, Phys. Rev. Lett. **99**, 107401 (2007).
[17] L. Peng, L. Ran, H. Chen, H. Zhang, J. A. Kong, and T. M. Grzegorczyk, Phys. Rev. Lett. **98**, 157403 (2007).
[18] S. Y. Liu, W. K. Chen, J. J. Du, Z. F. Lin, S. T. Chui, and C. T. Chan, Physi. Rev. Lett. **101**, 157407 (2008).
[19] K. Vynck, D. Felbacq, E. Centeno, A. I. Cabuz, D.

Cassagne, and B. Guizal, Phys. Rev. Lett. **102**, 133901 (2009).
[20] J. J. Du, S. Y. Liu, Z. F. Lin, J. Zi, and S. T. Chui, Phys. Rev. A **79**, 051801(R) (2009).
[21] G. S. Blaustein, M. I. Gozman, O. Samoylova, I. Y. Polishchuk, and A. L. Burin, Opt. Express **15**, 17380, (2007).
[22] Y. Fink, J. N. Winn, S. Fan, C. Chen, J. Michel, J. D. Joannopoulos, and E. L. Thomas, Science **282**, 1679 (1998).
[23] E. Yablonovitch, Phys. Rev. Lett. **58**, 2059 (1987).
[24] S. John, Phys. Rev. Lett. **58**, 2486 (1987).
[25] H. C. van de Hulst, *Light Scattering by Small Particles* (Dover, New York, 1981).
[26] Z. Ruan and S. Fan, Phys. Rev. Lett. **105**, 013901 (2010).
[27] I. Botten, M. S. Craiga, R. C. McPhedranb, J. L. Adamsc, and J. R. Andrewartha, Optica Acta, **28**, 413 (1981).
[28] P. Sheng, R. S. Stepleman, and P. N. Sanda, Phys. Rev. B **26** 2907 (1982).
[29] A. Tishchenko, Optical and Quantum Electronics **37**, 309 (2005).
[30] V. Karagodsky, F. Sedgwick, and C. Chang-Hasnain, Opt. Express **18**, 16973 (2010).
[31] A. Rahman, K. Vasilev, and P. Majewski, J. Opt. Soc. Am. B **28**, 2919 (2011).
[32] A. Devilez, B. Stout, and N. Bonod, Phys. Rev. B **81**, 245128 (2010).
[33] K. B. Crozier, E. Togan, E. Simsek, and T. Yang, Opt. Express **15**, 17482 (2007).
[34] S. T. Chui, S. Y. Liu and Z. F. Lin, J. Phys. Condens. Matter **22**, 182201 (2010).
[35] F. D. M. Haldane and S. Raghu, Phys. Rev. Lett. **100**, 013904 (2008).
[36] Z. Wang, Y. D. Chong, J. D. Joannopoulos, and M. Soljacic, Phys. Rev. Lett. **100**, 013905 (2008).
[37] Z. Wang, Y. D. Chong, J. D. Joannopoulos, and M. Soljacic, Nature **461**, 772 (2009).
[38] Y. Poo, R. X. Wu, Z. F. Lin, Y. Yang, and C. T. Chan, Phys. Rev. Lett. **106**, 093903 (2011).